Paper Reference No 227

Compact Gas-Solid Insulating Systems for High-Field-Stress in HVDC applications

M.TENZER, V. HINRICHSEN
Technische Universität Darmstadt
Germany

A. WINTER, J. KINDERSBERGER
Technische Universität München
Germany

D. IMAMOVIC
Siemens AG
Germany

ABSTRACT

When designing compact gas-solid insulating systems for use under high direct voltages, special attention has to be paid to the electric field distribution, in particular its transient behavior. After energizing an insulating system with a direct voltage, the initial capacitive electric field distribution on the insulators changes towards a stationary resistive distribution. The capacitive-resistive field transition goes hand in hand with the development of surface charges on solid-gas interfaces. Charges travel along the electric field lines through the gas, the solid material or along insulator surfaces and accumulate due to the low conductivity of the insulating material. The influence of surface charges may result in a significant reduction of the insulating strength during operation or in the case of polarity reversal of the applied voltage. Due to the fact that the duration of charge accumulation and decay and the stationary distribution of charge accumulations are mainly determined by the bulk and surface conductivity of the insulating material, the capacitive-resistive field transition and the stationary resistive field distribution may be controlled by modifying the electric properties of the solid insulating material. The influence of surface conductivity on the field transition and distribution is investigated using field calculations. For this purpose, a simulation model was developed, which takes into account the physical processes of conductivity in gases, i.e. a constant natural ionization rate, recombination and motion of charge carriers in the electric field and diffusion. The simulation results are in good agreement with measurements of the surface potential on epoxy resin insulators with untreated and with highly resistive coated surface.

With regard to the influence of the bulk conductivity of an insulating material system, experimental investigations of functionally filled epoxy resin material providing a well-controlled electrical conductivity are presented. This material offers a non-linear, field dependent conductivity that can be controlled in the production process of the fillers as well as by the preparation of the insulator specimens and may provide a fast decay of surface charges and an improved resistive field distribution. The field dependent surface and bulk conductivity of this material are determined on material probes. Resistive losses are moderate and cause only negligible thermal heating, which is considered an acceptable price for fast surface charge decay. Results of high-voltage tests in a gas insulated test vessel with direct and impulse voltage stress on real size test specimens are also presented in this contribution. So far, all experimental investigations show very promising results. Furthermore, the long term behavior of the material is investigated on material probes in accelerated ageing tests under combined electrical (direct voltage) and thermal stress.

KEYWORDS

HVDC, Insulators, Surface charge accumulation, Gas-Insulated, Functional Fillers

INTRODUCTION

After an insulation system is energized with a direct voltage, the initial capacitive field distribution is determined by the permittivity of the dielectrics. During voltage application, charges travel through the insulating materials and along interfaces between the dielectrics and accumulate on surfaces due to the differing conductivity of the involved materials. The accumulation of surface charges goes hand in hand with a transition of the field distribution from an initial capacitive to a stationary resistive state, which is determined by the volume and surface conductivity of the insulating materials (1). Not only the field distribution, but also the duration of the capacitive-resistive field transition depends on the dielectric and electrical properties of the dielectrics and may be in the order of weeks for highly insulating materials like epoxy resin (2). The insulation strength of gas-solid insulation systems may be reduced during operation or polarity reversal of the applied voltage by the influence of surface charges (3, 4, 5).

In order to design an insulation material optimized for direct voltage applications, hence to especially avoid the accumulation of charges on the insulators' surface and to achieve a faster transition to the stationary, resistive field distribution, the material properties have to be modified. The objective is an insulation material with an adjusted, well defined electrical conductivity κ of low temperature dependence, long term stable properties and that is suitable for high electric field stress.

In the case of gas-insulated, high-field applications, an electrical conductivity in the range of $\kappa = 10^{-12}…10^{-14}$ S/m (depending on insulator geometry and voltage level) has been determined as an optimum by simulation tools. The adjusted conductivity may feature both a fast surface charge decay within seconds and a fast transition from the capacitive to the stationary resistive field distribution as well as acceptably low electrical losses.

SIMULATION MODEL

Knowledge of the dielectric and electrical properties of the insulating materials is a crucial requirement for the calculation of the transient capacitive-resistive field transition. The volume and surface conductivity of polymeric insulation material is highly influenced by the temperature and humidity of a gas (6, 7). Besides possible sources like field emission from the cathode, micro discharges and partial discharges on particles, charge carriers in gas are mainly generated as a consequence of natural ionization i.e. photoionization due to cosmic and natural radiation (8, 9). The volume conductivity of gas is nonlinearly depending on the electric field strength according to a constant charge carrier generation rate (10). An average value of $\partial n_{\mathrm{IP}}/\partial t$ = 10 IP/(cm^{3}s) can be assumed for the ion pair generation rate in ambient air, although it is subject to fluctuations (11).

A physical gas model was developed that takes into account the generation, recombination and motion of charge carriers in a gas volume. The gas model is combined with the model of a solid insulator. The current density $\boldsymbol{J}_{\mathrm{I}}$ in the solid insulation material is defined by the equation of continuity (1):

$$\boldsymbol{J}_{\mathrm{I}} = \frac{\partial \boldsymbol{D}}{\partial t} + \kappa_{\mathrm{VI}} \cdot \boldsymbol{E} \qquad \text{equ. 1}$$

$\boldsymbol{D}$	electric flux density
κ_{VI}	volume conductivity of the solid insulating material
$\boldsymbol{E}$	electric field strength

Gas model

As a consequence of their high electron affinity, charges in insulating gases like SF_6 and air occur in form of gas ions (12). The dynamic change of the positive and negative ion density n^+ and n^- respectively is defined in form of transport equations (13):

$$\frac{\partial n^+}{\partial t} = \frac{\partial n_{\mathrm{IP}}}{\partial t} - k_{\mathrm{r}} \cdot n^+ \cdot n^- - div(n^+ \cdot b^+ \cdot \boldsymbol{E}) + D^+ \cdot \nabla^2 n^+ \qquad \text{equ. 2}$$

$$\frac{\partial n^-}{\partial t} = \frac{\partial n_{\mathrm{IP}}}{\partial t} - k_{\mathrm{r}} \cdot n^+ \cdot n^- + div(n^- \cdot b^- \cdot \boldsymbol{E}) + D^- \cdot \nabla^2 n^- \qquad \text{equ. 3}$$

k_r	recombination coefficient
b^+, b^-	mobility of positive/negative ions
D^+, D^-	diffusion coefficient of positive/negative ions

The electric field is described by the electric potential φ, which can be calculated in dependence of the space charge density ρ using the Poisson-equation:

$$\boldsymbol{E} = -grad(\varphi) \quad \text{equ. 4}$$

$$\nabla^2\varphi = -\frac{\rho}{\varepsilon} = \frac{e \cdot (n^+ - n^-)}{\varepsilon_0} \quad \text{equ. 5}$$

e	elementary charge
ε	permittivity of the gas
ε_0	electric constant

The diffusion coefficient is describes via the Einstein-equation (14):

$$D^{+/-} = b^{+/-} \cdot \frac{k \cdot T}{e} \quad \text{equ. 6}$$

k	Boltzmann constant
T	temperature

The current density through the gas $\boldsymbol{J}_G$ is the result of conduction and displacement current $\boldsymbol{J}_C$ and $\boldsymbol{J}_D$ respectively:

$$\boldsymbol{J}_G = \boldsymbol{J}_C + \boldsymbol{J}_D = \frac{\partial \boldsymbol{D}}{\partial t} + e \cdot \boldsymbol{E} \cdot (n^+ \cdot b^+ + n^- \cdot b^-) - e \cdot grad(D^+ \cdot n^+ - D^- \cdot n^-) \quad \text{equ. 7}$$

Surface conduction

Surface conduction of an insulator can be simulated by a thin layer with thickness d_L and volume conductivity κ_{VL}, resulting in a surface conductivity κ_S (15). The dynamic change of the surface conductivity σ_S can be calculated with (16):

$$\frac{\partial \sigma_S}{\partial t} = \frac{\partial D_{Gn}}{\partial t} - \frac{\partial D_{In}}{\partial t} = J_{In} - J_{Gn} - div(\kappa_S \cdot E_t) \quad \text{equ. 8}$$

$$\kappa_S = \kappa_{VL} \cdot d_L \quad \text{equ. 9}$$

D_{In}, D_{Gn}	normal component of the electric flux density on the insulator-side and the gas-side of the interface, respectively
J_{In}, J_{Gn}	normal component of the current density on the insulator-side and the gas-side of the interface, respectively
E_t	tangential component of the electric field strength

A thickness of d_L = 50 µm is used in all following simulations. The surface conductivity is varied by choosing different values of the volume conductivity κ_{VL} of the surface layer.

Boundary and starting conditions

Dirichlet-conditions are used to define the electric potential on the high voltage and ground electrode φ_{HV} and φ_{GND} respectively:

$$\varphi_{HV} = U \quad \text{equ. 10}$$

$$\varphi_{\mathrm{GND}} = 0 \qquad \text{equ. 11}$$

U applied voltage

The electric potential on the gaseous and the solid side of the insulator surface φ_{SG} and φ_{SI} respectively has to be continuous:

$$\varphi_{\mathrm{S}} = \varphi_{\mathrm{SG}} = \varphi_{\mathrm{SI}} \qquad \text{equ. 12}$$

φ_{S} surface potential

The charge carrier densities of positive and negative ions are defined in dependence of the direction of the current flow. If current flow occurs from a boundary, the value of the positive ion density and the normal component of the gradient of the negative charge carrier density are zero. If current flow occurs into a boundary, the value of the negative ion density and the normal component of the gradient of the positive charge carrier density are zero.

The electric potential everywhere in the field space at the time t_0 = 0 is zero. The charge carrier density at t_0 = 0 is in the equilibrium state, calculated in dependence of charge carrier generation and recombination:

$$n^+(t_0) = n^-(t_0) = \sqrt{\frac{\partial n_{\mathrm{IP}}}{\partial t} \cdot \frac{1}{k_{\mathrm{r}}}} \qquad \text{equ. 13}$$

Discontinuous Galerkin-method

Equations 2 to 5 and equation 8 are combined into a nonlinear inhomogeneous partial equation system. The equation system has to be solved using boundary and starting conditions and an iterative time dependent solver. The equation system is implemented in the FEM-program COMSOL Multiphysics. The continuous Galerkin-method (CGFEM) as the common solver method of FEM-software tends to create oscillations of the unknown variables and may lead to non-converging results if a dominating convective term appears in the equation system (17). Though, the equation system is implemented in weak formulation according to the discontinuous Galerkin-method (DGFEM), including terms for “interior penalty” and “upwind”-stabilization to support convergence of the numerical solver (18, 19).

EXPERIMENTAL SETUP

The surface potential is investigated on cylindrical insulators made from Al_2O_3-filled epoxy resin material with radius r_{I} = 40 mm and height h_{I} = 132 mm and embedded aluminium electrodes. The insulators are mounted between a plate-shaped ground and a high voltage electrode (**Figure 1**).

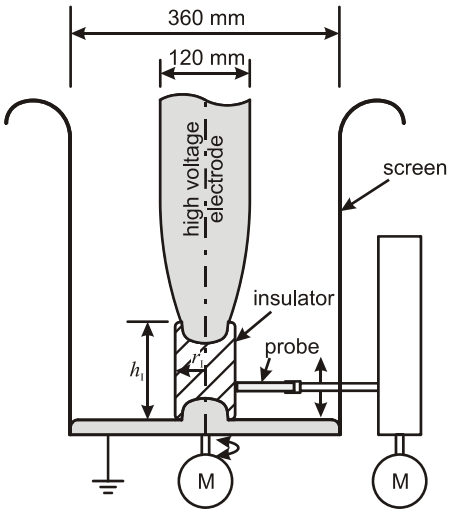

Figure 1: Electrode arrangement with cylindrical epoxy resin insulator and surface potential probe

The insulator and the high voltage electrode are surrounded by a grounded screen. An electrostatic voltmeter "Trek 341B", which uses the field compensation principle, is used for measurements of the surface potential. The contact-free probe is installed 2 mm in front of the insulator. Almost the entire insulator surface can be scanned moving the probe axially and rotating the insulator using stepper motors. Between two measurements, the probe is parked in a weak field area inside of the ground electrode. Measurements are performed under controlled conditions under air with a temperature ϑ = 20°C and relative humidity RH ≤ 2%.

The influence of surface conductivity is investigated using uncoated and coated insulators. The surface conductivity of uncoated insulators is assumed to be negligible. As coating, an insulating varnish is mixed with slightly conducting fillers. Before measurements, the insulators are dried at least for 48 h at a temperature ϑ = 100°C and stored afterwards at ϑ = 20°C and RH ≤ 2% for at least 24 h. After installation in the electrode arrangement, the insulator surface is cleaned with isopropanol. The absence of surface charges is checked by measurements of the surface potential without applied voltage.

SIMULATION RESULTS

A rotational symmetric model of the experimental setup is used for the simulations. Values of $\partial n_{\mathrm{IP}}/\partial t$ = 10 IP/(cm^{3}s) for the ion pair generation rate, b^+ = 1.36 cm^2/(Vs) and b^- = 1.87 cm^2/(Vs) for the mobility of positive and negative ions, respectively and k_{r} = 1.4×10^{-6} cm^3/s for the recombination coefficient of atmospheric air and volume conductivity of the solid epoxy resin material of κ_{VI} = 3.33×10^{-20} S/cm are assumed (7, 11, 20, 21). Starting at the time t_0 = 0 the direct voltage at the high voltage electrode is increased linearly within 100 ms from 0 to the value U. For investigations of the duration of the capacitive-resistive field transition the transition time $t_{90\%}$ is used. $t_{90\%}$ is defined as the time that is needed until the difference of the potential at the point i between the potential at the time $t_{90\%}$ $\varphi_{\mathrm{i}}(t_{90\%})$ and the stationary potential at the time t_∞ $\varphi_{\mathrm{i}}(t_\infty)$ is ≤ 10% of the initial potential difference:

$$\frac{|\varphi_{\mathrm{i}}(t_\infty) - \varphi_{\mathrm{i}}(t_{90\%})|}{|\varphi_{\mathrm{i}}(t_\infty) - \varphi_{\mathrm{i}}(t_0)|} \leq 0.1 \qquad \text{equ. 14}$$

After application of the direct voltage, charge carriers travel along the electric field lines and along the insulator surface and accumulate as a consequence of the differing volume conductivity of the gas and the solid insulating material and due to an inhomogeneous tangential component of the electric field strength. Hand in hand with charge carrier accumulation goes a change of the electric field distribution. The polarity and the distribution of the surface charge density on an insulator surface depends on the dominating charge carrier transport mechanism, i.e. transport through the solid or gaseous insulating material or along the insulator surface (22). **Figure 2** shows the surface charge density on a cylindrical epoxy resin insulator for different values of the surface conductivity.

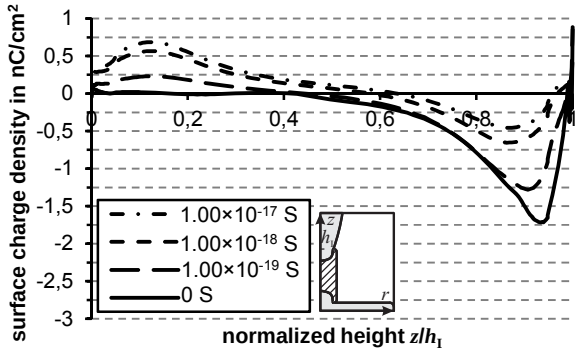

Figure 2: Simulated surface charge density along an insulator in the stationary resistive state for different values of the surface conductivity κ_{S}

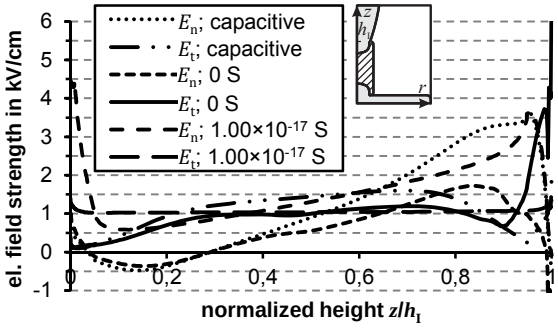

Figure 3: Simulated normal and tangential component of the electric field strength along an insulator (gaseous side) in the initial capacitive and stationary resistive state for different values of the surface conductivity κ_{S}

U = 15 kV; $\varepsilon_{\mathrm{rI}}$ = 5; κ_{VI} = 3.33×10^{-20} S/cm; $\partial n_{\mathrm{IP}}/\partial t$ = 10 IP/(cm^{3}s); b^+ = 1.36 cm^2/(Vs); b^- = 1.87 cm^2/(Vs); k_{r} = 1.4×10^{-6} cm^3/s

For negligible surface conductivity $\kappa_S = 0$ the surface charge distribution is dominated by charge carrier transport through the gas volume. Mostly negative ions accumulate on the insulator, reaching the surface along the electric field lines through the gas volume. The distribution of surface charges corresponds to the distribution of the normal component of the electric field strength E_n in the initial capacitive state after application of a direct voltage (**Figure 3**). E_n is influenced by the presence of surface charges and in the stationary resistive state E_n is significantly reduced at the gaseous side of the interface, i.e. the electric field distribution is changed in a way that the electric field lines run preferably in the gas. The tangential component of the electric field E_t isn't changed markedly. As a consequence of the negative surface charges, the surface potential is reduced on the whole insulator (**Figure 4**). The duration of the capacitive-resistive field transition differs along the insulator surface (**Figure 5**). The average value of $t_{90\%}$ is approx. 10 100 h for negligible surface conductivity.

For surface conductivity $\kappa_S \geq 1\times10^{-19}$ S, an influence of charge transport along the dielectric interface can be observed in the stationary resistive distribution of surface charges. For $\kappa_S = 1\times10^{-17}$ S the stationary surface charge distribution is dominated by surface conduction and does not change even for higher values of κ_S. The distribution corresponds to the distribution of the tangential component of the electric field in the initial capacitive state. The distribution of E_t along the insulator is changed in a way that an almost homogeneous distribution is reached in the stationary resistive state. The stationary distribution of the surface potential is almost linear. The duration of the capacitive-resistive field transition decreases for increasing values of surface conductivity because charges accumulate faster due to an increased surface current. The average value of $t_{90\%}$ decreases even for values $\kappa_S > 1\times10^{-17}$ S and is approx. 0.02 h for $\kappa_S = 1\times10^{-13}$ S.

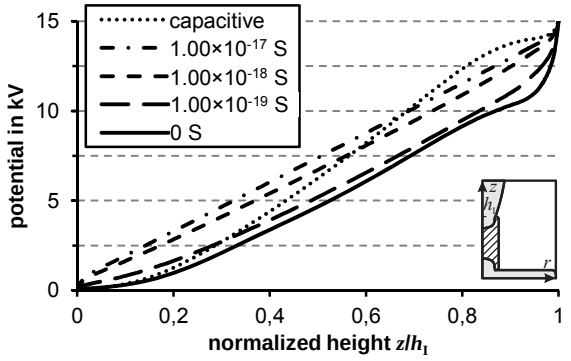

Figure 4: Simulated surface potential along an insulator in the initial capacitive and stationary resistive state for different values of the surface conductivity κ_S

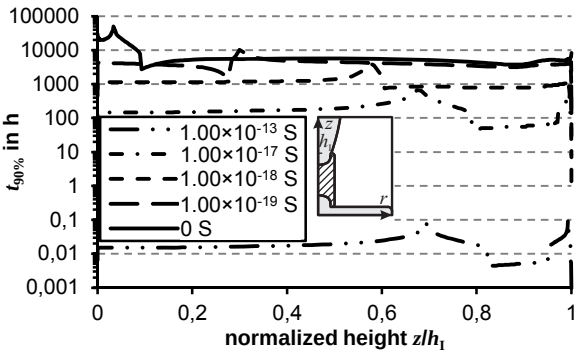

Figure 5: Simulated time $t_{90\%}$ along an insulator for different values of the surface conductivity κ_S

U = 15 kV; ε_{rI} = 5; κ_{VI} = 3.33×10^{-20} S/cm; $\partial n_{IP}/\partial t$ = 10 IP/(cm^{3}s); b^+ = 1.36 cm^2/(Vs); b^- = 1.87 cm^2/(Vs); k_r = 1.4×10^{-6} cm^3/s

SURFACE POTENTIAL MEASUREMENT

A direct voltage U = 15 kV is applied to the test setup. After energizing the insulation system, the potential is measured periodically on the insulator surface. Since the probe influences the electric field during a measurement, the feedback of the measuring system has to be taken into account in the analysis of the measurement results. Therefore, the distortion of the electric field during measurements is investigated using 3-dimensional field simulations and the influence of the probe is compensated in the measured results. The procedure is described in (22).

The measured surface potential along an uncoated insulator is shown in **Figure 6** in form of mean values around the insulators circumference for different times t after application of a direct voltage. The measurement results are compared to simulation results calculated with the gas model. A surface conductivity of the epoxy resin material of $\kappa_S = 1.00\times10^{-20}$ S is assumed, which is extrapolated from surface conductivity measurements at temperatures $\vartheta \geq 40$°C. The volume conductivity of the epoxy resin material at temperatures $\vartheta \leq 40$°C isn't in the measurable range of the available measuring systems, i.e. it has to be less than 1.00×10^{-18} S/cm. The ion pair generation rate inside of the test vessel is unknown, but it can be

assumed that it is less than 10 IP/(cm^{3}s) due to the shielding effect of the vessel material. For values $\partial n_{IP}/\partial t$ = 7 IP/(cm^{3}s) and κ_{VI} = 3.33×10^{-21} S/cm the measurement results match the simulation results considering the distribution and the temporal behaviour of the surface potential (**Figure 7**). After application of the direct voltage, negative gas ions accumulate on the insulator surface due to a dominating transport of charges through the gas. As a consequence, the surface potential on the insulator decreases. Although the stationary resistive state wasn't reached yet, the measurement was stopped after approx. 8 800 h. From the temporal development of the calculated surface potential it can be estimated, that the capacitive-resistive field transition would be finished after approx. 40 000 h.

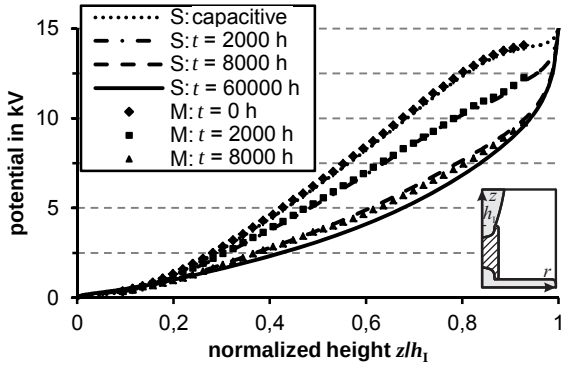

Figure 6: Simulation (S): Initial capacitive and stationary resistive surface potential along an uncoated insulator for different times t after application of a dc voltage;

Measurement (M): Mean values around the insulator's circumference corrected by the probe's influence along an insulator for different times t after application of a dc voltage

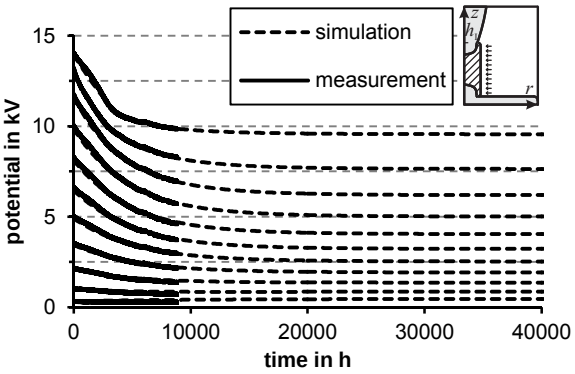

Figure 7: Simulation: Surface potential in different points on an uncoated insulator after application of a dc voltage;

Measurement: Mean values around the insulator's circumference corrected by the probe's influence in different points on an insulator after application of a dc voltage

Simulation: U = 15 kV; ε_{rI} = 5; κ_{VI} = 3.33×10^{-21} S/cm; κ_S = 1.00×10^{-20} S; $\partial n_{IP}/\partial t$ = 7 IP/(cm^{3}s); b^+ = 1.36 cm^2/(Vs); b^- = 1.87 cm^2/(Vs); k_r = 1.4×10^{-6} cm^3/s

Measurement: U = 15 kV; uncoated insulator; ϑ = 20°C; $RH \leq 2\%$

The surface potential along a coated insulator with a surface conductivity of approx. $\kappa_S \approx 9.10\times10^{-11}$ S is shown in **Figure 8**. As predicted by simulations, an almost linear distribution of the surface potential can be

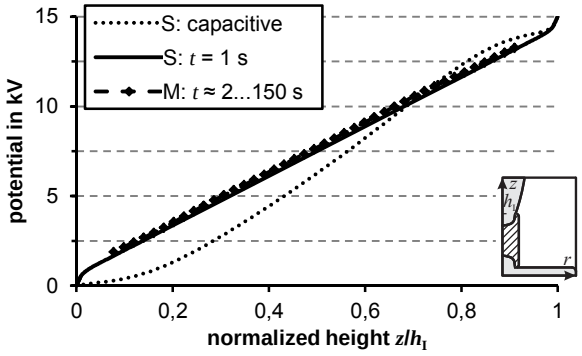

Figure 8: Simulation (S): Initial capacitive and stationary resistive surface potential along an coated insulator for different times t after application of a dc voltage; U = 15 kV; ε_{rI} = 5; κ_{VI} = 3.33×10^{-21} S/cm; κ_S = 9.10×10^{-11} S; $\partial n_{IP}/\partial t$ = 7 IP/(cm^{3}s); b^+ = 1.36 cm^2/(Vs); b^- = 1.87 cm^2/(Vs); k_r = 1.4×10^{-6} cm^3/s

Measurement (M): Mean values around the insulator's circumference along an insulator for different times t after application of a dc voltage; U = 15 kV; $\kappa_S \approx 9.10\times10^{-11}$ S, ϑ = 20°C; $RH \leq 2\%$

measured immediately after application of a direct voltage which doesn't change even after more than 48 h of voltage stress. As a consequence of the increased surface conductivity, the capacitive-resistive field transition is accelerated and the initial capacitive distributions can't be measured due to the limited motion speed of the measurement system. Simulations indicate that the stationary resistive state is reached after approx. 0.3 s. The measurement results aren't corrected by the influence of the probe, because the accumulation of surface charges isn't negligible slow compared to the duration of a measurement (approx. 2.5 min) (22). However, measurement results match simulation results because of the dominating surface conductivity.

FUNCTIONALLY FILLED EPOXY RESIN WITH ADJUSTED CONDUCTIVITY

Material Properties

Traditionally, several fillers, e.g. quartz flour or aluminum oxide are applied to epoxy resin based insulation materials, mainly for improving their mechanical properties. In polymer matrices, carbon black is often applied to achieve refractive or resistive field grading materials. However, the electrical conductivity of carbon black filled polymers is strongly dependent on the filling level and has a steep percolation curve in the region of the percolation threshold (23)

The objective is to use functional fillers having well defined intrinsic conductivity properties, which are relatively insensitive to the filling level in the epoxy resin matrix.

One possible type of such functional fillers is doped zinc oxide (ZnO) in the form of particles, known as microvaristors. The intrinsic electrical conductivity of microvaristors is mainly controlled by internal potential barriers at the primary grain boundaries (24). Various investigations on microvaristors showed a good reproducibility of the characteristics, but materials for high field strength are actually not commercially available. Prototype batches of "high-field" microvaristors showed the feasibility of these particles in general (25), as long as the high switching field strengths in the range of several kilovolts per millimetre are achieved just by the sintering process. If, however, smaller particle sizes shall be achieved by additional milling of the ZnO particles, the resulting insulator material shows instable long term behaviour under direct voltage stress (26). In conclusion, more development needs to be performed by the microvaristor manufacturers before "high-field-microvaristors" are ready for series production.

A new approach with another type of functional fillers (Minatec® functional fillers, in the following abbreviated with "MFF") is presented in detail in this contribution. These commercially available particles are flake-shaped mica pigments, covered by a thin tin oxide (SnO) layer doped with antimony (Sb) and titanium dioxide (TiO_2) (27). This nanoscaled metal oxide layer on the mica pigments provides a defined intrinsic

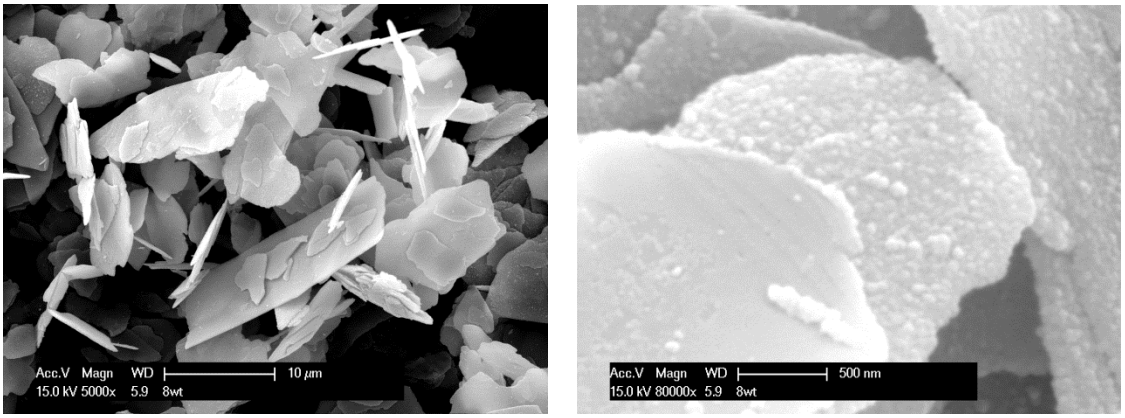

Figure 9: SEM records of the semiconducting mica pigments MFF. Left: Flake-shaped particles, right: Nanoscaled zoom showing the fine-grained metal oxide layer structure of the pigments.

nonlinear conductivity of the particles that can be adjusted over a wide range of conductivity κ and nonlinearity exponent α (27).In Figure 9, SEM records of the particles are shown. The very thin, flake-shaped MFF particles have a length of 5 µm to 20 µm and a very fine-grained metal oxide layer structure that can be seen in the zoom of the right hand part of the picture. Due to their special geometric shape of very thin flakes, the percolation threshold in coatings is reached at low filling degrees (27). For first basic investigations, MFF particles are filled into the whole volume of a polymer: The particles are mixed into a bisphenol A type epoxy resin at a filling degree of 38 % of weight and are vacuum-cast into a cylindrical mould with a height h = 130 mm and a diameter d = 45 mm.

Electrical Characterization of the Specimens

The bulk conductivity of MFF-filled epoxy resin specimens is determined by using a guarded electrode configuration according to IEC 60093 (28). The specimens are thin discs cut out from the manufactured cylindrical specimens. Electric contact is achieved by silver conductive painting on the end faces, and the bulk E-κ characteristic is recorded by using a direct voltage source and a picoampèremeter. All measurements are performed in a dry atmosphere temperature chamber at temperatures of ϑ = 30 °C, 60 °C and 100 °C ± 1 K. Results are plotted in Figure 10. Conductivity shows a relatively low variation with temperature and electrical field stress. Additionally, some of the manufactured specimens are prepared with an electrode configuration on their cylindrical circumference by silver conductive painting and aluminum electrodes, inspired by the IEC 60093 (28) standard method for surface resistivity measurements on tubes, see Figure 11 left. In this configuration only surface conductivity is measured. Currents in these investigations are considerably higher than those measured through the bulk of the specimen at ϑ = 100 °C and E = 1 kV/mm, as presented in the diagram of Figure 11right. The measured bulk current, indicated by the blue triangle, is 0.5 nA, whereas the measured surface current is 100 nA, (red circles), which is about 200 times higher. Because of the unknown current penetration depth in case of the surface current measurement method, conductivity $\kappa(E)$ cannot be calculated by this measurement. However, SEM records of the breaking edge of the investigated specimens can give a possible explanation of this phenomenon. In the upper half of Figure 12 the surface-near region is shown, where the included pigments are orientated in parallel to the surface, whereas on the lower half, being further allocated from the surface, the SEM record shows an arbitrarily distributed orientation of the pigments.

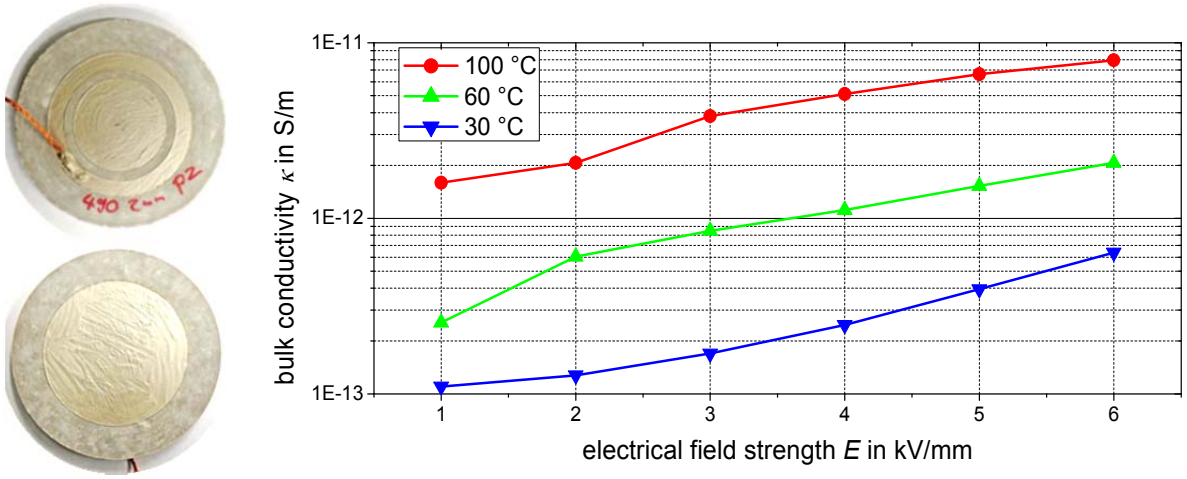

Figure 10, left: Specimen preparation for bulk conductivity measurement (discs of 2 mm height, diameter 45 mm) Right: Semi-logarithmic plot of the measured bulk conductivities $\kappa(E,\vartheta)$ at three different temperatures (ϑ = 30 °C, 60 °C and 100 °C), recorded in a dry atmosphere temperature chamber.

Due to the exclusively parallel orientation of the particles directly near the surface (caused by the molding process) the number of potential barriers along the conduction path is lower and thus overall surface

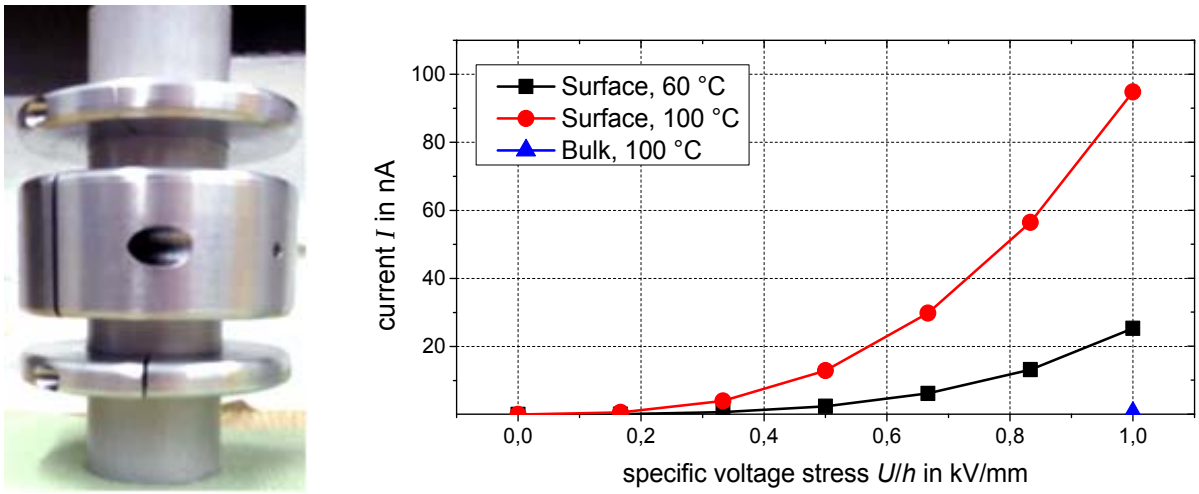

Figure 11, left: Electrode configuration for the surface measurements. The cylinder surface (under the electrodes) is prepared with silver conductive painting in order to provide good electrical contact. Gap between the electrodes: 10 mm. Right: Currents measured on the surface of the cylindrical specimens at two different temperatures (ϑ = 60 °C and 100 °C), recorded in a dry atmosphere temperature chamber. The blue triangle represents the measured current value of the bulk at ϑ = 100 °C and E = 1 kV/mm.

conductivity is higher. To prove this assumption, the cylindrical specimens' surface is machined and approx. two millimeters of the material are removed. Afterwards, the specimen is again contacted with silver conductive painting and the electrodes. The conductivity measurement is repeated in this new configuration, and the measured currents are significantly lower, reaching a level similar to that of the measured bulk currents.

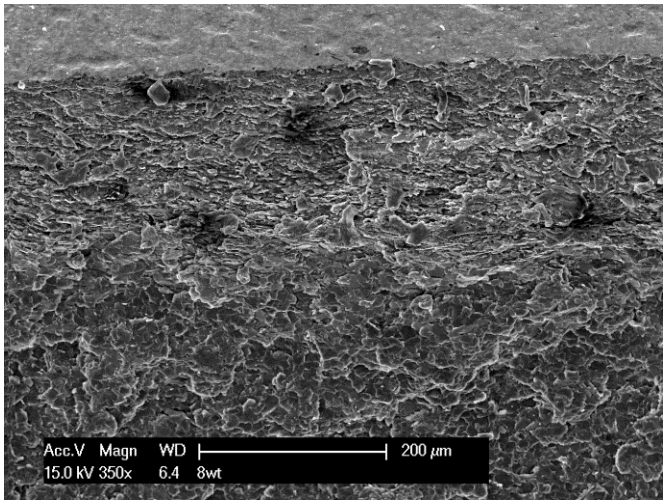

Figure 12: SEM record of the surface-near breaking edge of a MFF-filled epoxy resin specimen. In the upper region of the record, the pigments are oriented in parallel to the surface, whereas they are oriented arbitrarily in the inner bulk region in the lower region of the record

High Voltage Investigations

For the high voltage investigations, the manufactured cylinders (height h = 125 mm, diameter d = 45 mm) are contacted with silver conductive painting on their end faces and finally mounted between aluminum electrodes in a gas-insulated test vessel under SF_6 gas. The test voltage is applied through an air-gas bushing. Current measurements via a picoampèremeter are performed at the specimens' low voltage side. The test voltage is gradually increased in steps of ΔU = 20 kV every 300 seconds, and the measured current

is recorded. Differing from the results of the material characterization, the current takes higher values in the µA-range when U = 150 kV (respectively U/h = 1.2 kV/mm) is reached.

Based on the measured results, the theoretical model, presented in Figure 13, may explain the differing current ranges. The left hand model highlights the active tangential bulk resistances (violet resistances $R_{b,t}$) and represents the bulk measurement method with the results presented in Figure 10. The middle picture takes into account only the surface-nearest tangential resistances $R_{s,t}$, which are contacted by the silver conductive painting in the investigations that lead to the results shown in Figure 11. Caused by the particles' special geometry and the nonlinear conductive metal oxide layer, the material has anisotropic electrical characteristics, in other words: the surface-near normal resistances $R_{s,n}$ are expected to be much higher than the tangential resistances $R_{s,t}$. Hence, only a very limited current penetration of the normal resistances $R_{s,n}$ in series with the surface-near tangential resistances $R_{sn,t}$ from the outer surface to the inner layers is assumed. This is expressed in Figure X5 middle by the light green and light blue resistances. The right hand model represents the specimen investigated in the high voltage setup. As the end faces are completely covered with silver conductive painting, all the tangential resistances $R_{b,t}$, $R_{sn,t}$ and $R_{s,t}$ are actively involved in current transport.

However, in order to statistically validate these results, further specimens and other specimen geometries have to be investigated.

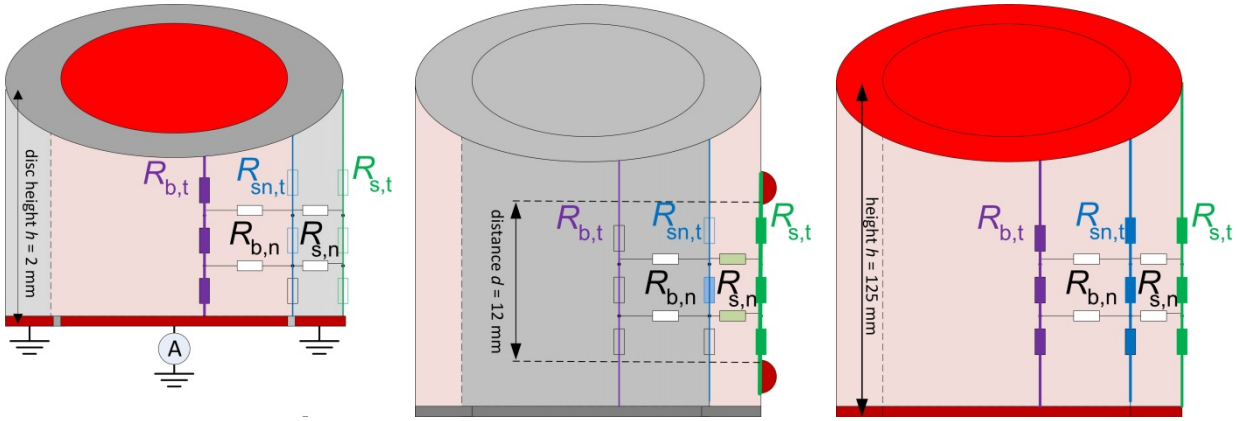

Figure 13: Theoretical model for the resistive conduction paths of the manufactured specimens at the different experimental investigations. The electrodes are colored in red. Left: Bulk conductivity measurement of disc specimen (the tangential bulk resistances $R_{b,t}$ shown in violet are dominating the conductivity), Middle: Surface conductivity measurement of cylindrical specimen (the tangential surface resistances $R_{s,t}$ shown in green are dominating the surface conductivity and presumably lesser involved (caused by anisotropy) also the normal resistances $R_{s,n}$ near to the surface in series with surface-near resistance $R_{sn,t}$), Right: High voltage experiment with cylindrical specimen (all the tangential resistances $R_{b,t}$, $R_{sn,t}$ and $R_{s,t}$ are conducting the measured total current I)

Long Term Investigations

For long term investigations, a test setup consisting of three heating chambers, one high direct voltage power supply and automated measurement systems is used. To change the polarity, the smoothing capacitor of the hv d,c, source is discharged within 17 seconds. Afterwards the circuit is re-energized at opposite polarity. The specimens are mounted in heating chambers providing forced convection. The direct voltage is fed into the chambers by bushings. Following magnitudes are measured and controlled, respectively: current through and voltage across the specimens, temperature and relative humidity inside the chamber. Five of the disc shaped specimens are tested in each of the three heating chambers. The temperatures are chosen as follows: ϑ = 30 °C, 60 °C, 100 °C. Again, the electrical contacts of the specimens are implemented as electrodes according to IEC 60093 (28) for bulk conductivity measurements, by using silver conductive painting.

In a first long term test of 1000 h time duration, all specimens at 30 °C and 60 °C show a stable d.c. behavior. This can be seen exemplarily for two of the tested specimens in Figure 14.

Interestingly, polarization is apparently not faster at 60 °C, even though the conductivity is obviously higher. Obviously, the still decreasing current after the first 150 hours is not only caused by polarization effects but also by other phenomena. A similar effect can be observed after the applied polarity reversals.

The specimens exposed to a temperature of 100 °C show less stable behavior. Reasons for this finding have to be further investigated. One possible reason may be the fact that the glass transition temperature of the filled epoxy resin polymer is expected to be only slightly higher than 100 °C.

It is actually not yet clear up to which values temperature acts as acceleration factor only, and when additional ageing effects are stimulated. Further investigations are required in order to establish a standard accelerated ageing test procedure for this class of material.

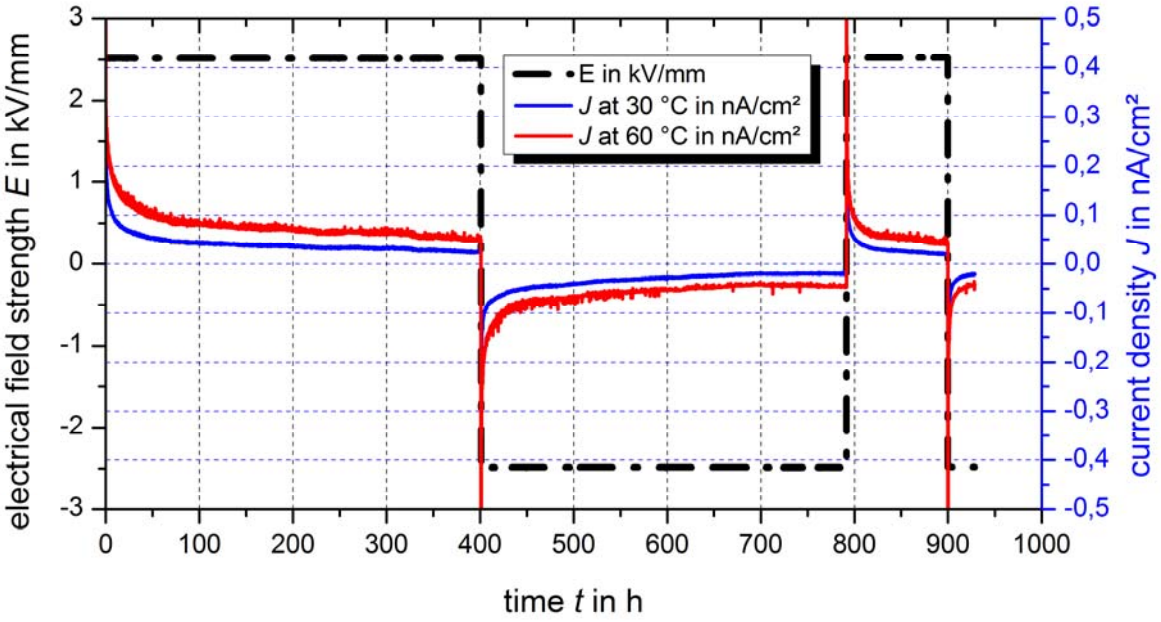

Figure 14: Results of the long term tests. The applied voltage is plotted in black. Polarity reversals were realized at t = 400 h, t = 800 h and t = 900 h. The applied electrical field strength E is plotted in black. The current density behavior over the time of two specimens is plotted in blue (Temperature 30 °C) and red (Temperature 60 °C).

CONCLUSION

The capacitive-resistive field transition and the stationary resistive field distribution in gas-solid insulation systems are connected to the accumulation of electric charges in dielectrics and on dielectric surfaces. Surface charges accumulate in dependency of the dominant charge transport mechanism through the solid insulating material, the gas and along dielectric surfaces, i.e. in dependency of the volume conductivity of an insulator and a gas and the surface conductivity of an insulator. A transient simulation model was developed which describes the conductivity of a gas by taking into account the generation, recombination and motion of charge carriers. The duration of the capacitive-resistive field transition can be influenced by varying the surface conductivity of an insulator. The simulation results are verified by measurements of the surface potential on uncoated insulators with negligible surface conductivity and highly resistant coated insulators.

Several investigations on epoxy resin specimens filled with functional fillers have clearly proven the feasibility of manufacturing functional-filled materials for high-field applications.

Microvaristors may be one possible solution that is ready-to-work for lower electrical field strength but which has to be further developed for higher electrical field strength applications.

MFF filled epoxy resin shows very promising results for high-field applications: Focused on the desired conductivity κ, the bulk characteristics are in the range that is required for high-field direct current insulating materials, and κ shows a comparatively low dependence of temperature. In several tests, high direct field strengths $E > 6$ kV/mm were successfully applied to the specimens. In a first long term test at moderate electric field stress ($E = 2.5$ kV/mm), all specimens have shown stable direct current behaviour at 30 °C and 60 °C. A further test at higher electric field stress ($E = 4$ kV/mm) has already been started, and the specimens show stable characteristics so far.

The electrical properties of the filled epoxy resin are anisotropic. It must, therefore, be strictly differentiated between surface and bulk characteristics. In order to achieve fast surface charge decay, the higher surface conductivity may be exploited.

Finally, it should be noted that the particles used for the investigations are not yet optimized for this special high-field insulator application. The material parameters conductivity κ and nonlinearity exponent α can be adjusted in a certain range to better adopt the characteristics to the intended application. Further investigations with modified particles optimized for this high-field application have already been started in cooperation with the particle manufacturer.

ACKNOWLEDGEMENT

The authors wish to express their gratitude to Dr. Reinhold Rüger (Merck KGaA, Performance Materials, Darmstadt, Germany) for the lively exchange of ideas and for providing different batches of functional particles for practical investigations.

REFERENCES

(1) A. J. Schwab, “Field Theory Concepts”, Springer-Verlag, Berlin, Germany, 1981
(2) F. Messerer, “Gas-Insulated Substations (GIS) for HVDC”, doctoral thesis, TU München, Germany, 2001
(3) E. K. Volpov, “Dielectric Strength Coordination and Generalized Spacer Design Rules for HVAC/DC SF6 Gas Insulated Systems”, IEEE Trans. on Dielectr. Electr.Insul., Vol. 11, No. 6, pp. 949 – 963, 2004
(4) H. Fujinami, T. Takuma, M. Yashima, T. Kawamoto, “Mechanism and Effect of DC Charge Accumulation on SF6 Gas Insulated Spacers”, IEEE Trans. Power Del., Vol. 4, No. 3, pp. 1765 – 1782, 1989
(5) S. Kumara, “Electrical Charges on Polymeric Insulator Surfaces and their Impact on Flashover Performance”, doctoral thesis, Chalmers University of Technology, Sweden, 2012
(6) B. Lutz, J. Kindersberger, “Influence of the relative humidity on the DC potential distribution of polymeric cylindrical model insulators”, Proceedings of the 2010 International Conference on Condition Monitoring and Diagnosis, paper C4-4, pp. 541 – 544, Tokyo, Japan, 2010
(7) B. Lutz, J. Kindersberger, “Determination of Volume Resistivity of Polymeric Insulators by Surface Charge Decay”, Proceedings of the 16th International Symposium on High Voltage Engineering, paper A-4, pp. 1 – 6, Johannesburg, South Africa, 2009
(8) C. M. Cooke, “Charging of Insulator Surfaces by Ionization and Transport in Gases”, IEEE Trans. Electr. Insul., Vol. EI-17, No. 2, pp. 172 – 178, 1982
(9) A. Knecht, „Das Isolationssystem Schwefelhexafluorid-Feststoffisolator bei Gleichspannungsbelastung“, doctoral thesis, ETH Zürich, Switzerland, 1984
(10) J. Kindersberger, C. Lederle, “Surface Charge Decay on Insulators in Air and Sulfurhexafluorid – Part I: Simulation”, IEEE Trans. Dielectr. and Electr. Insul., Vol. 15, No. 4, pp. 941 - 948, 2008
(11) J. A. Chalmers, “Atmospheric Electricity”, Pergamon Press, London, New York, Paris, 1957
(12) N. Wiegart, L. Niemeyer, F. Pinnekamp, W. Boeck, J. Kindersberger, R. Morrow, W. Zaengl, M. Zwicky, I. Gallimberti and S. A. Boggs, “Inhomogeneous Field Breakdown in GIS - The Prediction of Breakdown Probabilities and Voltages - Part II: Ion Density and Statistical Time Lag”, IEEE Trans. Power Del., Vol. 3, pp. 931 - 938, 1988
(13) S. A. Boggs, N. Wiegart, “Influence of Experimental Conditions on Dielectric Properties of SF6 - Insulated Systems – Theoretical Considerations”, in “Gaseous Dielectrics IV” edited by L. G. Christophorou and M. O. Pace, Pergamon Press, New York, USA, pp. 531 - 539, 1984
(14) L. I. Sirotinski, „Hochspannungstechnik – Band 1: Gasentladungen“, VEB Verlag Technik, Berlin, Germany, 1955
(15) H. Singer, “Feldberechnung mit Oberflächenleitschichten und Volumenleitfähigkeit der Isolation”, etz-Archiv, VDE-Verlag, Berlin Offenbach, Germany, Vol. 3, No. 8, pp. 265 – 267, 1981
(16) E. Volpov, “Electric Field Modeling and Field Formation Mechanism in HVDC SF6 Gas Insulated Systems”, IEEE Trans. Dielectr. Electr. Insul., Vol. 10, No. 2, pp. 204 – 215, 2003
(17) E. H. Georgoulis, “Discontinuous Galerkin Methods on Shape-Regular and Anisotropic Meshes”, doctoral thesis, University of Oxford, 2003

(18) D. A. Di Pietro, A. Ern, “Mathematical Aspects of Discontinuous Galerkin Methods”, Springer-Verlag, Berlin, Germany, 2012
(19) B. Rivière, “Discontinuous Galerkin Methods for Solving Elliptic and Parabolic Equations - Theory and Implementation”, Soc. for Industr. and Appl. Math., Philadelphia, USA, 2008
(20) H. A. Erikson, “On the Nature of the Ions in Air and in Carbon Dioxide”, Physical Review, Vol. 24, No. 5, pp. 502 – 509, 1924
(21) S. McGowan, “Ion-Ion Recombination in Laboratory Air”, Physics in Med. and Bio., Vol. 10, No. 1, pp. 25 – 40, 1965
(22) A. Winter, J. Kindersberger, “Stationary Resistive Field Distribution along Epoxy Resin Insulators in Air under DC Voltage”, IEEE Trans. Dielectr. and Electr. Insul., Vol. 19, No. 5, pp. 1732 – 1739, 2012
(23) V. Schuell, H. Schäufele: „Carbon Blacks für leitfähige Kunststoffe“. ETG Workshop „Werkstoffe mit nichtlinearen dielektrischen Eigenschaften“, 2008, Stuttgart, Germany.
(24) L. Donzel, F. Greuter, Th. Christen: “Nonlinear Resistive Electric Field Grading Part 2: Materials and Applications”. IEEE Electrical Insulation Magazine, Vol. 27, No. 2, 2011, pp. 18-29.. 5, pp. 1732 – 1739, 2012
(25) M. Tenzer, V. Hinrichsen: “Investigations on Microvaristors as Functional Fillers in Insulation Systems for HVDC Applications”. ISH 2011, August 22nd - 26nd 2011, Hannover, Germany, ISBN 978-3-8007-3364-4
(26) M. Tenzer, M. Secklehner, V. Hinrichsen: „Short and long term behavior of functionally filled polymeric insulating materials for HVDC insulators in compact gas insulated systems”. 23rd Nordic Insulation Symposium, June 9-12 2013, Trondheim, Norway, ISBN 978-82-321-0274-7
(27) R. Rüger: “Halbleitende Metalloxid-Pigmente mit nichtlinearen elektrischen Eigenschaften”. 5. RCC Fachtagung, 3.+4. Mai 2012, Berlin, Germany.
(28) IEC 60093, “Methods of test for volume resistivity and surface resistivity of solid electrical insulating materials” 2nd edition, 1980.

Biographical Details of Authors:

Dipl.-Ing. Michael Tenzer was born in 1981 in Bensheim (Germany) and studied electrical engineering at the Technische Universität Darmstadt in Germany. He received his diploma in 2009. Since 2009 he is working as research assistant at the Department of High Voltage Laboratories of Technische Universität Darmstadt.

Prof. Dr.-Ing. Volker Hinrichsen studied and graduated in High Voltage Technology at the Technische Universität Berlin, Germany. From 1989 to 2001 he was with Siemens PTD H, Berlin. From 1992 to 2001, he was director R&D for surge arresters. Since 2001 he is full professor at Technische Universität Darmstadt, Germany, Department of Electrical Engineering and Information Technologies, head of the High-Voltage Laboratories. He is active in IEC (Chairman of TC 37), a Member of Cigré, IEEE and VDE and Vice Chair of VDE/ETG.

Dipl.-Ing. Axel Winter was born in Munich, Germany in 1982. He received the Dipl.-Ing. degree in electrical engineering from the Technische Universität München, Germany in 2008. From 2008 to 2013 he worked as research assistant at the Laboratory of High Voltage Technology and Power Transmission of the Technische Universität München, investigating the performance of electrical insulation systems under dc voltage stress. Since 2013, he has been development engineer with the Tyco Electronics Raychem GmbH, in Ottobrunn/Munich.

Prof. Dr.-Ing. Josef Kindersberger received the Dipl.-Ing. and the Dr.-Ing. degrees from the Technische Universität München in 1979 and 1986, respectively. From 1986 to 1995 he was with the High Voltage Insulator Group of Hoechst CeramTec AG in Wunsiedel in various positions. In 1995 he became full professor at the Technische Universität Dresden. Since 2001 he has been head of the Laboratory of High Voltage Technology and Power Transmission of Technische Universität München, Germany. He is active in IEC (chairman of TC 36), CIGRE (chairman SC D1), IEEE and VDE/ETG.

Dr.-Ing. Denis Imamovic studied and graduated at Graz University of Technology, Austria. In 2011, he joined Siemens AG, Energy Sector in Erlangen, Germany, in 2011, where he was Product Lifecycle Manager for Compact DC Solutions. In April 2013 he became the head of the department “Compact DC Solutions”. He is a Member of Cigré, IEEE, OGE and OVE.